UC San Diego
UC San Diego Previously Published Works

Title

AIBP protects against metabolic abnormalities and atherosclerosis[S]

Permalink

https://escholarship.org/uc/item/2x2048c8

Journal

Journal of Lipid Research, 59(5)

ISSN

0022-2275

Authors

Schneider, Dina A
Choi, Soo-Ho
Agatisa-Boyle, Colin
et al.

Publication Date

2018

DOI

10.1194/jlr.m083618

Copyright Information

Peer reviewed

AIBP protects against metabolic abnormalities and atherosclerosis[S]

Dina A. Schneider,* Soo-Ho Choi,* Colin Agatisa-Boyle,* Laurence Zhu,[†] Jungsu Kim,* Jennifer Pattison,* Dorothy D. Sears,*,[§] Philip L. S. M. Gordts,* Longhou Fang,[†] and Yury I. Miller[1],*

Departments of Medicine* and Family Medicine and Public Health,[§] University of California at San Diego, La Jolla, CA 92093; and Center for Cardiovascular Regeneration, Department of Cardiovascular Sciences,[†] Houston Methodist Research Institute, Houston, TX 77030

ORCID ID: 0000-0002-5276-3304 (D.A.S.)

Abstract Apolipoprotein A-I binding protein (AIBP) has been shown to augment cholesterol efflux from endothelial cells and macrophages. In zebrafish and mice, AIBP-mediated regulation of cholesterol levels in the plasma membrane of endothelial cells controls angiogenesis. The goal of this work was to evaluate metabolic changes and atherosclerosis in AIBP loss-of-function and gain-of-function animal studies. Here, we show that $Apoa1bp^{-/-} Ldlr^{-/-}$ mice fed a high-cholesterol, high-fat diet had exacerbated weight gain, liver steatosis, glucose intolerance, hypercholesterolemia, hypertriglyceridemia, and larger atherosclerotic lesions compared with $Ldlr^{-/-}$ mice. Feeding $Apoa1bp^{-/-} Ldlr^{-/-}$ mice a high-cholesterol, normal-fat diet did not result in significant differences in lipid levels or size of atherosclerotic lesions from $Ldlr^{-/-}$ mice. Conversely, adeno-associated virus-mediated overexpression of AIBP reduced hyperlipidemia and atherosclerosis in high-cholesterol, high-fat diet-fed $Ldlr^{-/-}$ mice. Injections of recombinant AIBP reduced aortic inflammation in $Ldlr^{-/-}$ mice fed a short high-cholesterol, high-fat diet. Conditional overexpression of AIBP in zebrafish also reduced diet-induced vascular lipid accumulation. In experiments with isolated macrophages, AIBP facilitated cholesterol efflux to HDL, reduced lipid rafts content, and inhibited inflammatory responses to lipopolysaccharide.jlr Our data demonstrate that AIBP confers protection against diet-induced metabolic abnormalities and atherosclerosis.— Schneider, D. A., S-H. Choi, C. Agatisa-Boyle, L. Zhu, J. Kim, J. Pattison, D. D. Sears, P. L. S. M. Gordts, L. Fang, and Y. I. Miller. **Apolipoprotein A-I binding protein protects against metabolic abnormalities and atherosclerosis.** *J. Lipid Res.* **2018.** 59: 854–863.

Cardiovascular disease (CVD) is a leading cause of morbidity and mortality in the United States, accounting for approximately one-third of all US deaths (1). Therapy to reduce LDL cholesterol (LDL-C) has led to remarkable improvement in clinical outcomes, decreasing the incidence of acute cardiovascular events by 25–35% (2, 3). Statins, ezetimibe, and recently apoB antisense and PCSK9 monoclonal antibodies all target plasma LDL-C as a major atherogenic factor. However, improving the other arc of cholesterol homeostasis—reverse cholesterol transport and atheroprotective HDL—has proven to be a challenging task. Results of clinical trials of cholesteryl ester transfer protein inhibitors put in doubt the efficacy of simply raising HDL cholesterol (HDL-C) levels as an ultimate therapeutic goal (4). Although HDL-C clearly correlates with atheroprotection in epidemiology studies, the current consensus in the cardiovascular field underscores the added importance of improving the functionality of HDL (5–8). However, in vivo mechanisms regulating HDL function are not sufficiently understood.

Our recent work and the work of others have highlighted apolipoprotein A-I binding protein (AIBP), which augments cholesterol efflux from endothelial cells (9, 10) and macrophages (11) to HDL. AIBP is a secreted protein discovered in a screen of proteins that physically associate with apoA-I (12). Human *APOA1BP* mRNA encoding AIBP is ubiquitously expressed, with the highest expression in kidney, heart, liver, thyroid gland, adrenal gland, and testis (12). AIBP is found in cerebrospinal fluid and urine and in plasma of patients with sepsis (12). The human *APOA1BP* gene is located at 1q21.2-1q22 on chromosome 1, which corresponds to the 1q21-q23 locus for familial combined

hyperlipidemia, a common multifactorial and heterogeneous dyslipidemia predisposing to premature coronary artery disease (13). Yet, there are no studies directly linking AIBP polymorphism with dyslipidemia or risk of CVD.

AIBP does not bind cholesterol or induce cholesterol efflux in the absence of HDL or apoA-I, but it does increase the turnover of HDL and thus accelerates cholesterol efflux (9). The goal of this work was to evaluate metabolic changes and atherosclerosis in AIBP loss-of-function and gain-of-function animal studies. We report that AIBP deficiency exacerbates weight gain, hyperlipidemia, and atherosclerosis, while overexpression of AIBP is protective against vascular lipid accumulation, atherosclerosis, and metabolic abnormalities.

MATERIALS AND METHODS

Animals and diets

All animal experiments were conducted according to protocols approved by the Institutional Animal Care and Use Committee of the University of California at San Diego. Mice were housed up to five per standard cage at room temperature and maintained on a 12:12 h light:dark cycle, with lights on at 07:00. Both food and water were available ad libitum. Wild-type C57BL/6 and $Ldlr^{-/-}$ mice were initially purchased from the Jackson Laboratory (Bar Harbor, ME) and bred in-house for experiments. $Apoa1bp^{-/-}$ mice on a C57BL/6 background were generated in our group as previously described (10) and cross-bred with $Ldlr^{-/-}$ mice. $Apoa1bp^{-/-}Ldlr^{-/-}$ mice develop and breed normally. For metabolic studies, mice on a C57BL/6 background were fed a high-fat diet (HFD; Research Diets D12451; supplemental Table S1) containing 45% kcal from fat, starting at age 10 weeks. For metabolic and atherosclerosis studies, mice on an $Ldlr^{-/-}$ background were fed either a Western diet (Teklad TD.96121; supplemental Table S2) containing 42% kcal from fat (21% milkfat) and 1.25% cholesterol or a high-cholesterol, normal-fat diet (Teklad TD.97131; supplemental Table S3) containing 1% cholesterol, starting at age 8 weeks.

Adult zebrafish were maintained at 28°C on a 14 h light/10 h dark cycle as previously described (14) and fed brine shrimp twice a day. Zebrafish larvae were fed Golden Pearls (Brine Shrimp Direct, Ogden, UT) twice a day, starting from 5 days postfertilization (dpf). The transgenic *hsp70:apoa1bp-2A-mRFP* zebrafish was generated by using constructs and methods previously described (9, 15, 16). The self-cleavage 2A peptide allows for expression of two separate proteins in the same tissue, with mRFP serving as an indicator of successful protein expression. Transgene expression was initiated by single or repeated heat shocks (transferring zebrafish for 1 h into water warmed to 37°C) and detected via mRFP fluorescence. Expression of the zebrafish Apoa1bp protein was confirmed in Western blot with a guinea pig polyclonal anti-zebrafish Apoa1bp antibody (9). For vascular lipid deposit experiments, Golden Pearls supplemented with 4% (wt/wt) cholesterol and 1 μg/g TopFluor Cholesterol (Avanti Polar Lipids) were fed to zebrafish from 5 to 15 dpf as described (15). Zebrafish were imaged by using a Nikon A1 confocal microscope, and images were analyzed as described (15).

Cohort sizes and blinding

Cohort sizes for experiments involving $Apoa1bp^{-/-}$ mice, which were considered the major goal of the study, were calculated based on an assumption that the difference between means would be 1.3- to 2.0-fold, with SDs of 10–50% of mean, depending on experiment; 80% power; and $P < 0.05$. Animals were assigned to respective groups randomly within genotype. Individuals performing atherosclerosis analysis were not informed of genetic background or hypothesis.

Glucose, insulin, and glucose tolerance test

Glucose tolerance test was performed at 8 weeks of diet feeding and 18 weeks of age. Mice on the C57BL/6 background were fasted 4 h prior to testing. Glucose was administered to mice at a dose of 1 g per kg of body weight via ip injection of 25% dextrose in sterile saline (VetOne). Blood was collected from tail at times 0, 10, 30, 60, 90, and 120 min, and blood glucose was measured on a OneTouch Ultra glucose monitor. Additional blood was collected into heparinized capillary tubes at times 0 and 10 min for measurement of plasma insulin via ELISA (Alpco; catalog no. 80-INSMSH-E01). In cohorts of mice on the $Ldlr^{-/-}$ background, plasma was isolated from terminal blood, and plasma glucose levels were measured by using a kit from Crystal Chem (catalog no. 81692) and insulin levels by using an ultrasensitive insulin ELISA (Alpco; catalog no. 80-INSMSU-E01).

Lipids and lipoprotein profile

Blood was collected from mice into EDTA tubes upon euthanization, and plasma was collected following centrifugation. Lipoprotein profiles were determined by pooling plasma from each genotype and quantifying cholesterol content of each fraction via fast protein liquid chromatography with a Superose 6 column.

Atherosclerosis studies

Atherosclerosis was assessed as previously described (17). Briefly, en face atherosclerosis was quantified via computer-assisted image analysis (ImagePro) of Sudan-stained whole aorta. Aortic root atherosclerosis was quantified by cutting cross-sections starting from the aortic origin until the last leaflet. Sections were stained with a modified Van Gieson stain, and lesion area was quantified via computer-assisted image analysis (ImagePro).

Cells

RAW264.7 cells were cultured in DMEM (Cellgro) supplemented with 10% heat-inactivated FBS (Omega Scientific) and 50 μg/ml gentamicin (Omega Scientific).

Western blot

Cell and tissue lysates were subjected to gel electrophoresis and immunoblot as described (18). Antibodies were purchased from Cell Signaling Technology: p65 (catalog no. 4767), phospho-p65 (catalog no. 3033), ERK1/2 (catalog no. 4695), phospho-ERK1/2 (catalog no. 9101), and GAPDH (catalog no. 2118).

Quantitative PCR

Total RNA was isolated by using Nucleospin RNA columns (Clontech). Isolated RNA was reverse-transcribed by using RNA to cDNA EcoDry (Clontech) following the manufacturer's protocol. Quantitative PCR (qPCR) was performed by using a KAPA SYBR FAST Universal qPCR kit (KAPA Biosystems, KK4602), with primers ordered from Integrated DNA Technologies and a Rotor Gene Q thermocycler (Qiagen). Primer sequences are listed in supplemental Table S4.

Recombinant AIBP

AIBP was produced in a baculovirus/insect cell system to allow for posttranslational modification and to ensure endotoxin-free preparation. Human AIBP was cloned into a pAcHLT-C vector

behind the polyhedrin promoter. The vector contained an N-terminal His-tag to enable purification and detection. Insect Sf9 cells were transfected with BD BaculoGold Baculovirus DNA and the AIBP vector. After 4–5 days, the supernatant was collected to afford a baculovirus stock. Fresh Sf9 cells were infected with the AIBP-producing baculovirus; cell pellets were collected after 3 days, lysed, sonicated, and cleared by centrifugation; and the supernatants were loaded onto a Ni-NTA agarose column and eluted with imidazole. Protein was dialyzed against PBS, and the concentration was measured. Aliquots were stored at −80°C.

LPS/Kdo2-LipidA

In vitro experiments were conducted with Kdo2-LipidA (Avanti Polar Lipids), a well-characterized active component of lipopolysaccharide (LPS) and a highly specific Toll-like receptor 4 (TLR4) agonist (19). In text and figure legends, we refer to Kdo2-LipidA as LPS.

Adeno-associated virus 2-AIBP

Mouse AIBP (25–283 aa) was fused with fibronectin secretion sequence (FIB) at the N terminus and 6X-His at the C terminus (FIB-AIBP-His). FIB-AIBP-His was cloned into the pAAV-MCS vector (Agilent Technologies). All clones were sequenced to confirm the presence of the insert. Adeno-associated virus (AAV)-293 cells (Agilent Technologies) were transfected with 20 μg each of pAAV-FIB-AIBP-His, pAAV2 (Agilent Technologies), and pHelper DNA (Agilent Technologies) following the routine calcium phosphate-based protocol (Agilent Technologies). Subsequent steps of virus harvest, purification, and storage were according to published protocols (20). Viral DNA was extracted from purified virus, and the number of gene copies (gc) was determined by using qPCR with primers for the inverted terminal repeats (Takara Bio Inc.). Testing the FIB-AIBP-His plasmid and the AAV2-FIB-AIBP-His, we found that infected HEK 293 cells expressed AIBP of the correct molecular mass, recognized by anti-His (ThermoFisher, catalog no. MA1-21315). For AAV2-mediated AIBP expression, $Ldlr^{-/-}$ mice were iv injected with empty virus or AAV2-AIBP at 1×10^{12} gc per mouse. At 3 weeks postinjection, mice were fed a Western diet (Teklad TD.96121) for an additional 16 weeks. Testing for the expression of FIB-AIBP-His, liver was homogenized in RIPA buffer, and lysates were analyzed in Western blot.

White adipose tissue FACS

Flow cytometry of white adipose tissue (WAT) was performed as previously described (21). In brief, mice were euthanized, and tissue was perfused with PBS. WAT was minced in 5% BSA Dulbecco's PBS and centrifuged to remove erythrocytes and free leukocytes. Tissue was dissociated by using collagenase (Sigma C6885), filtered, and separated from adipocytes via centrifugation. The stromal vascular fraction was used for FACS analysis. Antibodies used were CD11b-FITC (BD 553310), F4/80-APC (Ab Serotec MCA497APC), and CD11c-PE (BD 553802).

Cholesterol efflux and lipid raft assays

A cholesterol efflux assay was performed as described (22, 23), with modifications. In brief, RAW264.7 cells were loaded with 2 μCi/ml [^{3}H]cholesterol (American Radiolabeled Chemicals), and cholesterol efflux was initiated by the addition of efflux medium containing 25 μg/ml HDL, in the presence or absence of 0.2 μg/ml recombinant AIBP, for 4 h. Background, nonspecific release of [^{3}H]cholesterol was measured in the absence of HDL. After incubation, the medium was collected and counted in a liquid

scintillation counter LS 6500 (Beckman Coulter). The cells were extracted with 2-propanol, and the lipid extract was added to ScintiVerse BD Cocktail (Fisher) and counted. Cholesterol efflux was expressed as a percentage of [^{3}H] counts in the medium compared with combined [^{3}H] counts in the cells and the medium. In these experiments, to replicate in vivo conditions, cells were not treated with a liver X receptor agonist or acyl-CoA cholesterol acyltransferase inhibitor.

For lipid raft measurements, RAW264.7 macrophages were incubated with FITC-conjugated cholera toxin B (CTB; Sigma) for 1 h on ice. Cells were washed two times with a FACS buffer, fixed with 3.7% formaldehyde for 15 min on ice, washed three times with a FACS buffer, and analyzed by using a FACSCanto II (BD Biosciences) flow cytometer.

Statistical analyses

Results were analyzed by using Student's *t*-test (for differences between two groups), one-way ANOVA (for multiple groups), or two-way ANOVA with the Bonferroni post hoc test (for multiple groups time course experiments), using GraphPad Prism. Differences between groups with $P < 0.05$ were considered statistically significant. Values were excluded if determined to be a significant outlier via the extreme studentized deviate test.

RESULTS

Metabolic abnormalities in $Apoa1bp^{-/-}$ mice

Systemic $Apoa1bp$ knockout mice have been developed in our laboratory as described (10). C57BL/6 and $Apoa1bp^{-/-}$ mice were fed a high-fat, normal-cholesterol diet (HFD) for 10 weeks starting from the age of 10 weeks. Despite having similar weights prior to diet feeding, $Apoa1bp^{-/-}$ mice were significantly heavier than their wild-type counterparts following the diet, despite consuming equivalent amounts of food (**Fig. 1A**, B). $Apoa1bp^{-/-}$ mice also exhibited impaired glucose clearance and increased circulating plasma insulin levels when subjected to a glucose tolerance test (Fig. 1C–E). Flow cytometry analysis of the WAT stromal vascular fraction revealed that epididymal WAT from $Apoa1bp^{-/-}$ mice contained a greater proportion of F4/80+CD11b+CD11c+ proinflammatory macrophages (Fig. 1F). Overall, $Apoa1bp^{-/-}$ mice exhibited more hallmarks of metabolic disease than their wild-type counterparts when fed a HFD.

Similar to HFD-fed $Apoa1bp^{-/-}$ mice, $Apoa1bp^{-/-} Ldlr^{-/-}$ mice fed a Western diet (high-fat, high-cholesterol) for 12 weeks became significantly heavier than $Ldlr^{-/-}$ mice (**Fig. 2A**). The livers of $Apoa1bp^{-/-} Ldlr^{-/-}$ mice had increased cholesterol and triglyceride content (Fig. 2B, C). Liver expression of TNFα mRNA was increased nearly 3-fold in $Apoa1bp^{-/-} Ldlr^{-/-}$ mice, suggesting increased liver inflammation (Fig. 2D). Plasma levels of glucose and insulin trended higher in terminal blood of nonfasted $Apoa1bp^{-/-} Ldlr^{-/-}$ mice (supplemental Fig. S1A, B).

AIBP deficiency results in exacerbated hyperlipidemia and atherosclerosis

$Apoa1bp^{-/-} Ldlr^{-/-}$ mice fed a Western diet had higher plasma cholesterol and triglyceride levels, primarily due
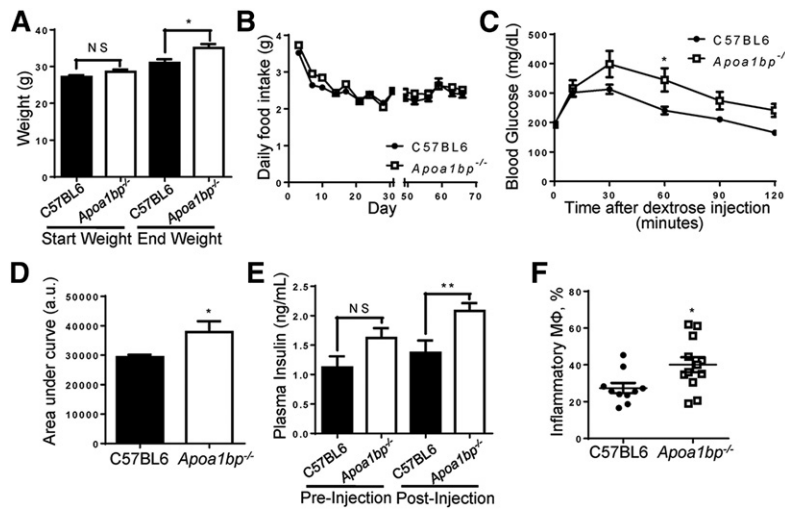
Fig. 1. Mice lacking AIBP exhibit metabolic abnormalities. C57BL/6 and $Apoa1bp^{-/-}$ mice were fed a HFD containing 45% (kcal) fat for 10 weeks starting at age 10 weeks. A: Mice were weighed at the start and completion of the diet (Student's *t*-test). B: Food intake was measured twice a week for the duration of the 10 week feeding period, with an interruption (X-scale break) while mice were moved and housed for metabolic testing. Prior to metabolic testing, mice were group-housed, and measurements given are based upon cage averages. No error bars are shown during the period for this reason. Following metabolic testing, all animals were individually housed, and measurements given represent the average of all individual mice. Error bars are only shown for the singly housed time period and are SEM. C: Glucose tolerance test. At week 8 of HFD feeding, mice were injected with dextrose solution, and blood was collected at time points shown (two-way ANOVA with Bonferroni's post hoc test). D: Integrated glucose levels (area under the curve from C; Student's *t*-test). a.u., arbitrary units. E: Insulin levels during glucose tolerance test at times 0 and 10 min (Student's *t*-test). F: Upon euthanization at 10 weeks of feeding, WAT was harvested from mice. Cells in the isolated stromal vascular fraction were characterized by FACS analysis. Inflammatory macrophages were defined as F4/80+CD11b+CD11c+ (Student's *t*-test). Mean ± SEM; n = 10–12; ** $P < 0.01$; * $P < 0.05$; NS, not significant differences.

to elevated VLDL and LDL, as compared with $Ldlr^{-/-}$ mice (**Fig. 3A**–D). Importantly, atherosclerotic lesions in the aortic root were significantly larger in $Apoa1bp^{-/-} Ldlr^{-/-}$ mice compared with $Ldlr^{-/-}$ mice (Fig. 3E–G). Overall, mice lacking AIBP had significantly increased weight gain, lipid levels in both plasma and liver tissue, and atherosclerosis when fed a high-fat, high-cholesterol diet.

However, feeding $Apoa1bp^{-/-} Ldlr^{-/-}$ mice a diet enriched in cholesterol (1%) but with normal fat content did not result in significant differences in weight, plasma cholesterol, triglycerides, glucose levels, or atherosclerosis when compared with $Ldlr^{-/-}$ mice (**Fig. 4** and supplemental Fig. S1C). Plasma insulin levels in $Apoa1bp^{-/-} Ldlr^{-/-}$ mice were higher than in $Ldlr^{-/-}$
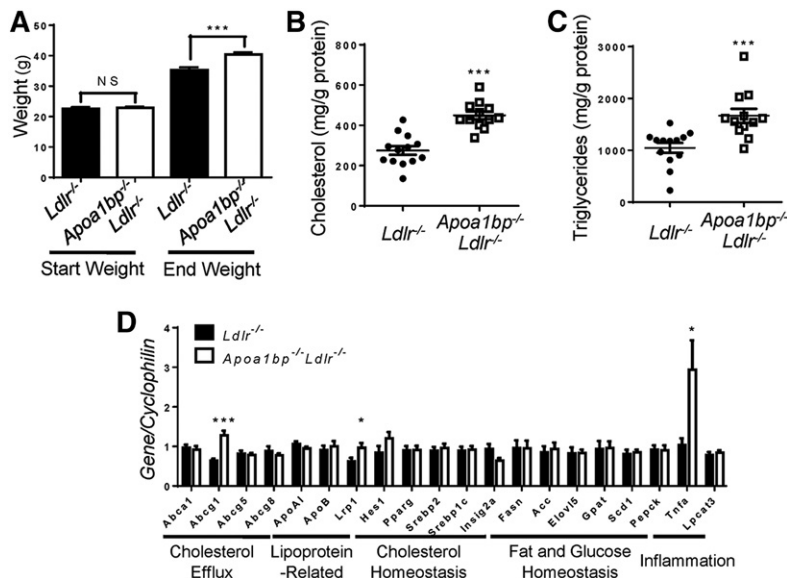

Fig. 2. Weight gain, liver lipid content, and gene expression profile in AIBP-deficient mice fed a Western diet. $Ldlr^{-/-}$ and $Apoa1bp^{-/-} Ldlr^{-/-}$ mice were fed a Western diet containing 1.25% cholesterol and 42% kcal from fat for 12 weeks starting from age 8 weeks. A: Mouse weights. B, C: Cholesterol content (B) and triglyceride content (C) in liver. D: Liver gene expression. Mean ± SEM; n = 12 or 13; *** $P < 0.001$; ** $P < 0.01$; * $P < 0.05$ (Student's *t*-test).
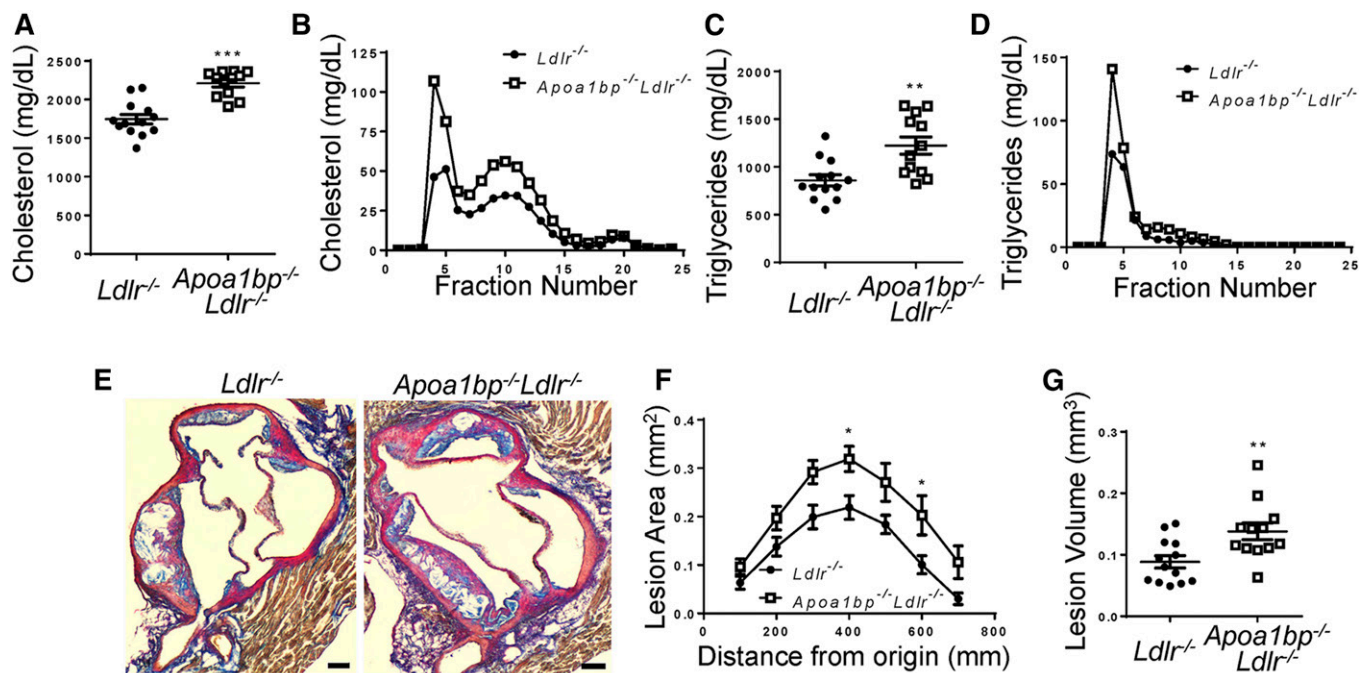
Fig. 3. Exacerbated hyperlipidemia and atherosclerosis in AIBP-deficient mice fed a Western diet. $Ldlr^{-/-}$ and $Apoa1bp^{-/-} Ldlr^{-/-}$ mice were fed a Western diet containing 1.25% cholesterol and 42% kcal from fat for 12 weeks starting from age 8 weeks. A–D: Plasma lipids at euthanization. Total cholesterol (A), cholesterol lipoprotein profile (B), total triglycerides (C), and triglyceride lipoprotein profile (D) (n = 12 or 13, Student's *t*-test) are shown. E: Representative images of aortic root from each genotype, at 0.3 mm from aortic valve origin. Scale bars, 100 μm. F: Aortic root atherosclerotic lesion size as a function of distance from first leaflet appearance (n = 12 or 13, two-way ANOVA with Bonferroni's post hoc test). G: Aortic root lesion volume (area under the curve from F; n = 12 or 13, Student's *t*-test). Mean ± SEM; *** $P < 0.001$; ** $P < 0.01$; * $P < 0.05$.

mice, but absolute numbers remained low (supplemental Fig. S1D). These results suggest the importance of AIBP-mediated metabolic changes in the development of atherosclerosis in the context of high-fat, high-cholesterol diets.

AAV-mediated expression of AIBP reduces weight gain, hyperlipidemia, and atherosclerosis

Next, we tested if sustained overexpression of mouse AIBP can reduce atherosclerosis. We generated an AAV2 with the FIB-AIBP-His construct. The fibronectin signal
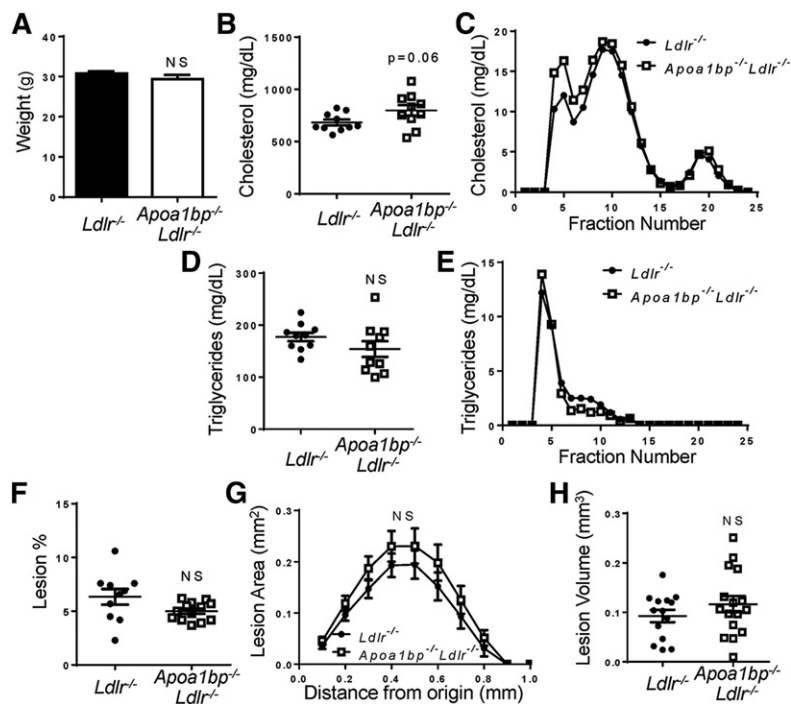

Fig. 4. Unchanged weight gain, hyperlipidemia, and atherosclerosis in AIBP-deficient mice fed a high-cholesterol, normal-fat diet. $Ldlr^{-/-}$ and $Apoa1bp^{-/-} Ldlr^{-/-}$ mice were fed a 1% cholesterol, normal-fat diet for 16 weeks starting from age 8 weeks. A: Weight at the time of euthanization (n = 10; Student's *t*-test). B–E: Plasma lipids at euthanization. Total cholesterol (B), cholesterol lipoprotein profile (C), total triglycerides (D), and triglyceride lipoprotein profile (E) (n = 10, Student's *t*-test) are shown. F: En face atherosclerotic lesions (n = 10; Student's *t*-test). G: Aortic root atherosclerotic lesion size as a function of distance from first leaflet appearance (n = 16; two-way ANOVA with Bonferroni's post hoc test). H: Aortic root lesion volume (area under the curve from G; n = 16, Student's *t*-test). Mean ± SEM; NS, not significant differences.

peptide (FIB) was inserted to ensure secretion of His-tagged mouse AIBP. Five-week-old $Ldlr^{-/-}$ mice were infected with AAV2-AIBP or the empty AAV2 (control) and, starting at 8 weeks of age, were fed a Western diet for 16 weeks. At the time of euthanization, livers were collected to confirm AIBP-His protein expression (supplemental Fig. S2); however, AIBP-His was not detectable in plasma. Both the control and AAV2-AIBP cohorts had similar weights prior to the start of the diet, but the mice overexpressing AIBP were significantly protected against diet-induced weight gain (**Fig. 5A**). Liver triglyceride levels were significantly lower and cholesterol levels trended lower in mice infected with AAV2-AIBP compared with the mice infected with the empty AAV2 (Fig. 5B, C). Plasma cholesterol levels had a trend toward reduction (Fig. 5D, E), and plasma triglycerides were significantly decreased (Fig. 5F, G). Importantly, there was a significant decrease in en face lesions (Fig. 5H), as well as a trend of reduced aortic root atherosclerosis in the AAV2-AIBP mice (Fig. 5I, J). Together, these data show protection against weight gain,

plasma lipid increases, and atherosclerosis by AAV-delivered AIBP.

Transgenic AIBP expression in zebrafish reduces diet-induced vascular lipid accumulation

We have previously described a hyperlipidemic zebrafish model in which vascular accumulation of lipid deposits was observed in live animals 10–14 days after initiation of high-cholesterol feeding (15, 24). To investigate whether AIBP can reduce lipid accumulation in the vasculature, we generated a transgenic zebrafish line in which expression of the *apoa1bp-2A-mRFP* construct is controlled by the *hsp70* heat shock promoter (**Fig. 6A**). Following protein expression, self-cleavage of the translated 2A peptide (16) released untagged zebrafish Apoa1bp and mRFP, the latter serving as a reporter for Apoa1bp expression. Heat shock-induced expression of the Apoa1bp protein was confirmed in Western blot (Fig. 6B). When zebrafish were fed a high-cholesterol diet (HCD) supplemented with fluorescently labeled cholesterol for 10 days, vascular lipid deposits
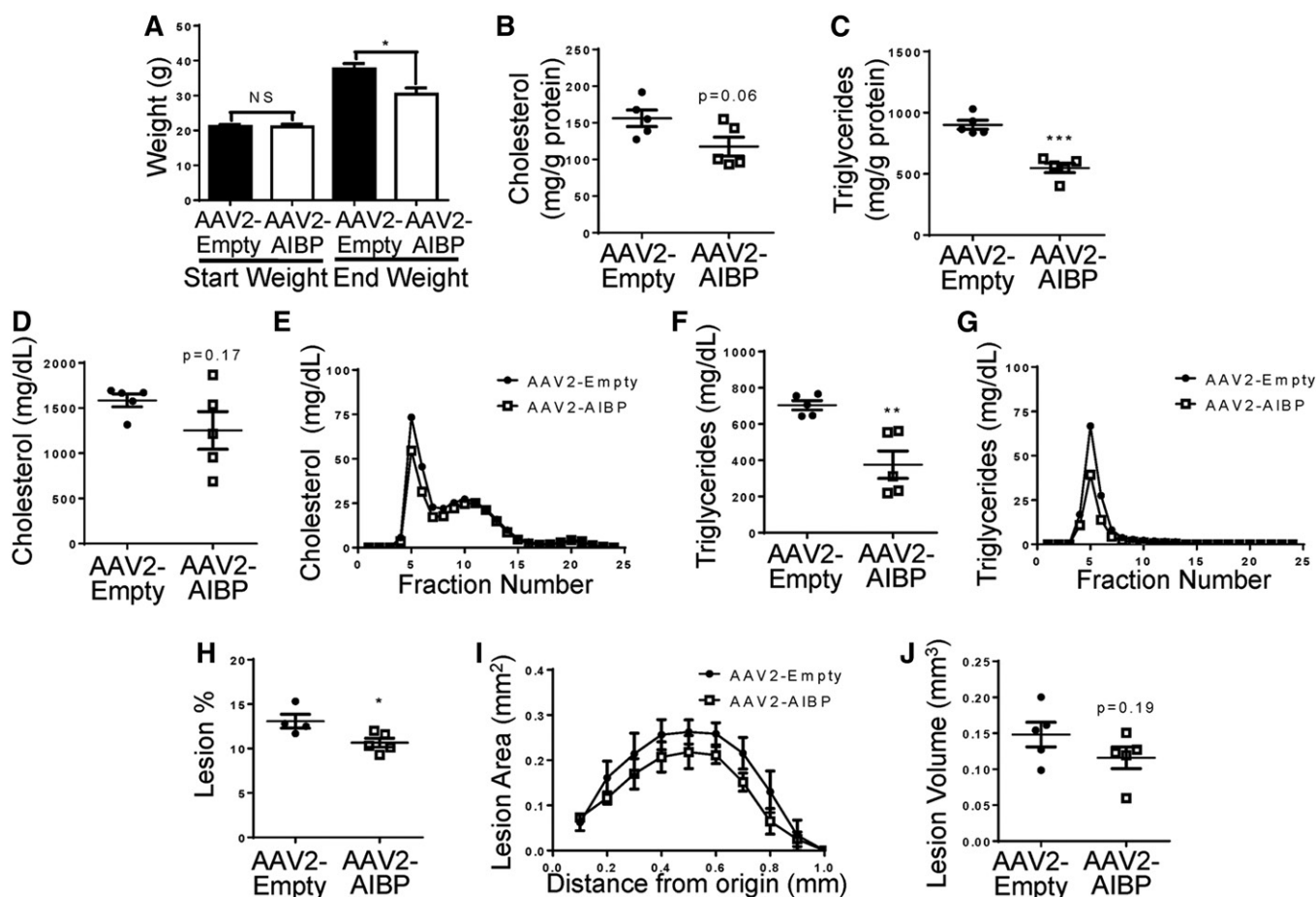

Fig. 5. Mice overexpressing AIBP are protected from weight gain, lipid abnormalities, and atherosclerosis. $Ldlr^{-/-}$ mice were injected with either AAV2-AIBP or the empty AAV2 and fed a Western diet containing 1.25% cholesterol and 42% (kcal) fat for 16 weeks starting from age 8 weeks. A: Mice were weighed at the start and completion of the diet (Student's *t*-test). B, C: Liver total cholesterol and triglyceride levels (Student's *t*-test). D, E: Plasma total cholesterol levels (Student's *t*-test) and the cholesterol lipoprotein profile. F, G: Plasma triglyceride levels (Student's *t*-test) and the triglyceride lipoprotein profile. H: Whole aorta en face lesion size (Student's *t*-test). I: Aortic root atherosclerotic lesion size as a function of distance from first leaflet appearance (two-way ANOVA with Bonferroni's post hoc test). J: Aortic root lesion volume (area under the curve from I; Student's *t*-test). Mean ± SEM; n = 5; *** $P < 0.001$; ** $P < 0.01$; * $P < 0.05$; NS, not significant differences.
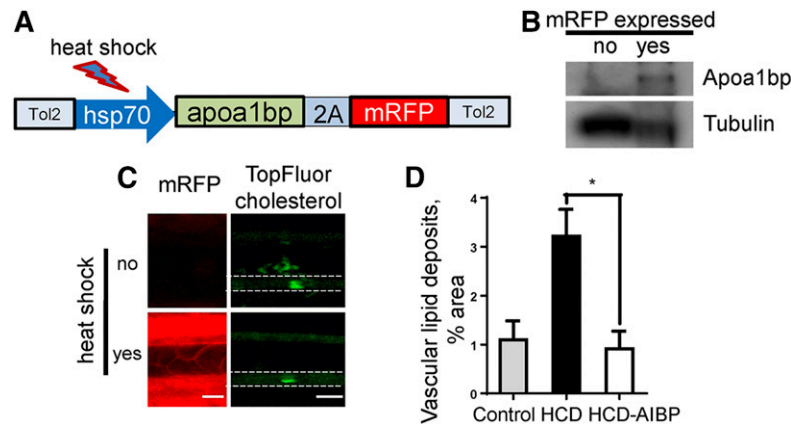
Fig. 6. Induced AIBP expression in zebrafish reduces diet-induced vascular lipid accumulation. A: Construct used to make transgenic *hsp70:apoa1bp-2A-mRFP* zebrafish. B: Heat shock-induced Apoa1bp protein expression. Embryos were subjected for 1 h to heat shock (37°C) at 1 dpf and again at 2 dpf. Three mRFP-negative and three mRFP-positive embryos were selected and homogenized in SDS-PAGE loading buffer. Lysates were run on SDS-PAGE, blotted, and probed with anti-zebrafish Apoa1bp and tubulin antibodies. C: Vascular lipid accumulation. Transgenic *hsp70:apoa1bp-2A-mRFP* zebrafish were fed control or 4% cholesterol diet supplemented with TopFluor-cholesterol for 10 days, and one group was subjected to three heat shock sessions during the 10-day feeding period. Left demonstrates heat shock-induced expression of mRFP (red) in zebrafish. Right shows vascular cholesterol deposits (green). White dashed lines trace the caudal vein in zebrafish. D: Quantification of vascular lipid deposits. Mean ± SEM; n = 4–11; * $P < 0.05$ (one-way ANOVA with Tukey's multiple comparison test).

increased significantly (Fig. 6C, D). Our previous work has shown that heat shock itself does not affect diet-induced vascular lipid accumulation (15). However, heat shock-induced overexpression of Apoa1bp prevented the HCD-induced increase in vascular lipid deposition (Fig. 6C, D), independently supporting the hypothesis that AIBP overexpression is atheroprotective.

Recombinant AIBP inhibits inflammatory responses by macrophages

Because AIBP was shown to augment HDL function (9, 10) and AIBP deficiency resulted in a higher liver expression of *Tnfa* (Fig. 2D), we hypothesized that AIBP reduces inflammatory responses by macrophages. In cell culture experiments, recombinant AIBP significantly increased cholesterol efflux from RAW264.7 macrophages (**Fig. 7A**) and reduced lipid raft content as assessed by FACS analysis of CTB binding to cells (Fig. 7B). To test whether AIBP inhibits inflammatory signaling, RAW264.7 macrophages were stimulated with LPS, in the presence of AIBP or BSA control. LPS-induced phosphorylation of p65 and ERK1/2 in macrophages was significantly reduced in AIBP-treated cells (Fig. 7C–E). In addition, recombinant AIBP significantly reduced gene expression of inflammatory cytokines in macrophages that were stimulated with LPS+IFNγ, a common inflammatory, M1-like polarization signal (**Fig. 8**).

We next tested if injections of recombinant AIBP can reduce vascular inflammation in mice. Hyperlipidemic *Ldlr*^{−/−} mice that had been fed a Western diet for 4 weeks were injected three times during the final week of feeding
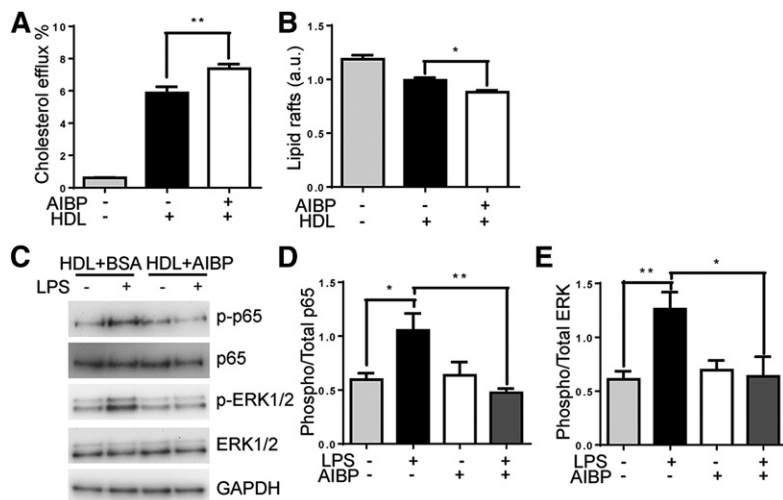

Fig. 7. AIBP facilitates cholesterol efflux and reduction in lipid rafts and inhibits macrophage inflammatory signaling. A: Cholesterol efflux from macrophages. RAW264.7 macrophages were loaded for 24 h with 2 μCi/ml [³H]cholesterol, and then efflux was stimulated by 25 μg/ml HDL treatment in the presence or absence of 0.2 μg/ml AIBP for 4 h (n = 14 for HDL-containing samples; n = 2 for media only). B: CTB binding was quantified via FACS to determine lipid raft content. RAW264.7 macrophages were loaded with acetylated LDL and treated for 4 h with media only or 25 μg/ml HDL in the presence or absence of 0.2 μg/ml AIBP or BSA (n = 3). a.u., arbitrary units. C: RAW264.7 macrophages were stimulated with 10 ng/ml LPS for 30 min, in the presence of BSA or AIBP. Phosphorylation of p65 and ERK1/2 were assessed via gel electrophoresis and Western blotting of cell lysates. D: Quantification of p65 phosphorylation (n = 5). E: Quantification of ERK phosphorylation (n = 6). Mean ± SEM; *** $P < 0.001$; ** $P < 0.01$; * $P < 0.05$ (one-way ANOVA).
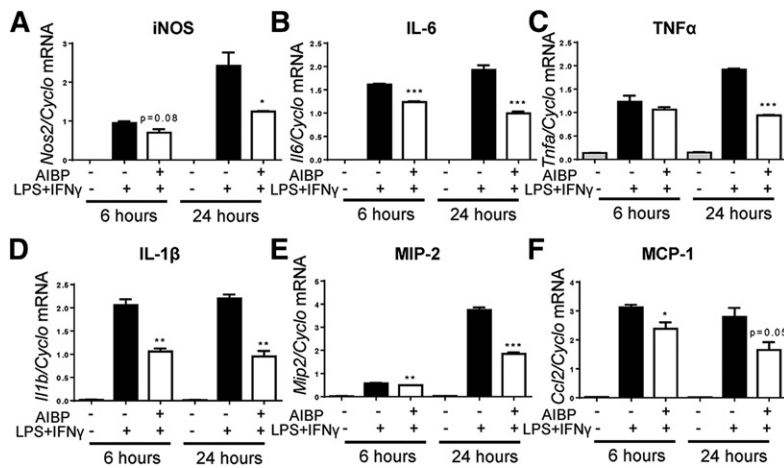
Fig. 8. AIBP suppresses macrophage inflammatory response. RAW264.7 macrophages were stimulated with 10 ng/ml LPS and 50 ng/ml IFNγ in the presence of 0.2 µg/ml BSA or AIBP, for 6 or 24 h. RNA was extracted from whole cell lysate. cDNA was synthesized from total RNA and used for qPCR to measure expression of *Nos2* (A), *Il6* (B), *Tnfa* (C), *Il1b* (D), *Mip2* (E), and *Ccl2* (F). Mean ± SEM; n = 3; *** $P < 0.001$; ** $P < 0.01$; * $P < 0.05$ (Student's *t*-test).

with PBS control, AIBP, or heat-inactivated AIBP. Injections did not affect mouse weight or plasma lipids (**Fig. 9A**–C). Aortas of these mice were used for total RNA isolation and gene expression analysis via qPCR. While heat-inactivated AIBP had no effect, nondenatured AIBP injection significantly reduced transcript levels of the inflammatory cytokines IL-6, IL-1β, and CCL2 compared with PBS-treated mice (Fig. 9D).

DISCUSSION

In this study, using loss-of-function and gain-of-function animal models, we explored the role of AIBP in metabolism and atherosclerosis. We found that $Apoa1bp^{-/-}Ldlr^{-/-}$ mice fed a Western diet had exacerbated liver steatosis, hyperlipidemia, and atherosclerosis. Conversely, AIBP gain-of-function resulted in reduced vascular lipid accumulation

Fig. 9. Injections of recombinant AIBP suppress vascular inflammation in vivo. $Ldlr^{-/-}$ mice were fed a Western diet containing 1.25% cholesterol and 42% (kcal) fat for 4 weeks and iv injected with PBS, 0.5 µg of AIBP, or 0.5 µg of heat-inactivated (HI)-AIBP three times during last week of feeding. A: Body weight. B: Total plasma cholesterol before the start of injections (week 3) and in terminal blood (week 4). C: Plasma triglycerides. D: mRNA expression of inflammatory cytokines in whole aorta. Mean ± SEM; n = 3 or 4; ** $P < 0.01$; * $P < 0.05$ (one-way ANOVA). NS, not significant differences.

in zebrafish and in reduced aortic inflammation, hyperlipidemia, and atherosclerosis in mice. These results suggest that AIBP restricts diet-induced metabolic abnormalities and is atheroprotective.

The results of our experiments demonstrate that the AIBP control of diet-induced metabolic abnormalities is an important factor in atheroprotection. Intravenous injections of recombinant AIBP into mice reduced hyperlipidemia-induced inflammation in the aorta, which is considered one of the earliest sites of diet-induced insulin resistance, preceding both liver and WAT (25). A sustained gain-of-function of AIBP, delivered via the AAV2-AIBP, resulted in protection against weight gain, hypertriglyceridemia, and atherosclerosis. Most tellingly, the AIBP knockout did not exacerbate atherosclerosis in the mice fed a normal-fat, high-cholesterol diet, which does not elicit a metabolic response in $Ldlr^{-/-}$ mice (26). However, when fed a HFD, $Apoa1bp^{-/-}$ mice gained more weight and were more glucose-intolerant than C57BL/6 mice, despite consuming equal quantities of food. Similarly, $Apoa1bp^{-/-}Ldlr^{-/-}$ mice fed a high-fat, high-cholesterol diet gained more weight and developed more severe hepatic steatosis compared with $Ldlr^{-/-}$ mice. The resulting exacerbation of hypertriglyceridemia and hypercholesterolemia led to more atherosclerosis in high-fat, high-cholesterol diet-fed $Apoa1bp^{-/-}Ldlr^{-/-}$ mice.

Interestingly, a recent study of mice with reduced expression of ABCA1 in adipocytes and macrophages (27) demonstrated that they share a similar phenotype of weight gain, increased plasma triglycerides, and increased liver cholesterol and triglyceride levels, as well as impaired glucose tolerance (28), found in the AIBP knockout mice. Increased fat mass and insulin resistance are linked to an increase in VLDL synthesis and a reduction in triglyceride-rich lipoprotein uptake (29, 30), both of which may contribute to the high VLDL plasma content in $Apoa1bp^{-/-}Ldlr^{-/-}$ mice. With greater exhibition of metabolic abnormalities, inflammatory macrophage signaling favored, and increased plasma cholesterol, it is expected that $Apoa1bp^{-/-}Ldlr^{-/-}$ mice have significantly increased prevalence of aortic root atherosclerosis.
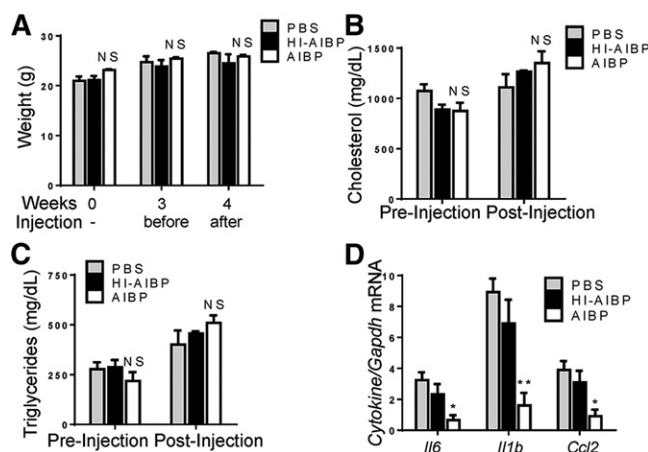
Systemic low-grade inflammation is an underlying cause of numerous pathologies, including the metabolic syndrome and atherosclerosis. A prevalent source of inflammatory cytokines are tissue macrophages, which become activated by danger-associated molecular patterns (DAMPs) arising in subjects consuming Western-type diets (31). Receptors for many DAMPs and inflammatory cytokines, such as TLR4 and IFNGR, reside in lipid rafts, which provide an ordered microenvironment for receptor dimerization and signaling complex assembly (32, 33). AIBP suppresses inflammatory signaling by enhancing cholesterol efflux from macrophages and thus depleting the lipid raft signaling platform. In AIBP knockout mice, the absence of AIBP results in an increase in the inflammatory milieu in the WAT and liver to propagate insulin resistance. In turn, lipids accumulate in the liver, and circulating VLDL levels increase. Excessive plasma VLDL leads to an increase in adipose triglycerides and mouse weight gain, as well as vascular lipid accumulation and atherosclerosis.

There are several limitations to our study. We considered only function of the secreted, extracellular AIBP. Several papers have been published proposing and testing intracellular functions of AIBP by using in vitro test tube assays (34–36). They suggest that intracellular AIBP may function as either an NAD(P)H-hydrate epimerase, often abbreviated as NAXE, or an ADP-ribosyltransferase, but so far, the in vivo significance associated with this enzymatic activity remains unclear. Yet, we cannot rule out the potential effects of intracellular AIBP on metabolic abnormalities in our mouse studies. However, we have shown ample evidence here that extracellular AIBP has an important role in regulating cholesterol efflux and lipid metabolism both in vitro and in vivo using animal models of gain-of-function of secreted or recombinant AIBP. Another consideration is that extracellular AIBP can have effects on multiple tissue types. Tissue-specific knockout of AIBP cannot address this issue in full, as AIBP may be secreted from an adjacent tissue. This is an important avenue for future research.

Using a variety of animal models, we have shown here that the addition of AIBP is atheroprotective, while conversely, the absence of AIBP is atherogenic. AIBP is highly conserved, acts at least in part extracellularly, and augments protective properties of HDL. Further exploration of atheroprotective properties of AIBP may help design future therapeutic interventions.∎

REFERENCES

1. Go, A. S., D. Mozaffarian, V. L. Roger, E. J. Benjamin, J. D. Berry, M. J. Blaha, S. Dai, E. S. Ford, C. S. Fox, S. Franco, H. J. Fullerton, C. Gillespie, S. M. Hailpern, J. A. Heit, V. J. Howard, M. D. Huffman, S. E. Judd, B. M. Kissela, S. J. Kittner, D. T. Lackland, J. H. Lichtman, L. D. Lisabeth, R. H. Mackey, D. J. Magid, G. M. Marcus, A. Marelli, D. B. Matchar, D. K. McGuire, E. R. Mohler, 3rd, C. S. Moy, M. E. Mussolino, R. W. Neumar, G. Nichol, D. K. Pandey, N. P. Paynter, M. J. Reeves, P. D. Sorlie, J. Stein, A. Towfighi, T. N. Turan, S. S. Virani, N. D. Wong, D. Woo, M. B. Turner, American Heart Association Statistics Committee, and Stroke Statistics Subcommittee. 2014. Heart disease and stroke statistics–2014 update: a report from the American Heart Association. *Circulation.* **129:** e28–e292.

2. Baigent, C., A. Keech, P. M. Kearney, L. Blackwell, G. Buck, C. Pollicino, A. Kirby, T. Sourjina, R. Peto, R. Collins, et al. 2005. Efficacy and safety of cholesterol-lowering treatment: prospective meta-analysis of data from 90,056 participants in 14 randomised trials of statins. *Lancet.* **366:** 1267–1278.

3. Steinberg, D., C. K. Glass, and J. L. Witztum. 2008. Evidence mandating earlier and more aggressive treatment of hypercholesterolemia. *Circulation.* **118:** 672–677.

4. Tall, A. R., and D. J. Rader. 2018. Trials and tribulations of CETP inhibitors. *Circ. Res.* **122:** 106–112.

5. Larach, D. B., E. M. deGoma, and D. J. Rader. 2012. Targeting high density lipoproteins in the prevention of cardiovascular disease? *Curr. Cardiol. Rep.* **14:** 684–691.

6. Fisher, E. A., J. E. Feig, B. Hewing, S. L. Hazen, and J. D. Smith. 2012. High-density lipoprotein function, dysfunction, and reverse cholesterol transport. *Arterioscler. Thromb. Vasc. Biol.* **32:** 2813–2820.

7. Rosenson, R. S., H. B. Brewer, W. S. Davidson, Z. A. Fayad, V. Fuster, J. Goldstein, M. Hellerstein, X. c. Jiang, M. C. Phillips, D. J. Rader, et al. 2012. Cholesterol efflux and atheroprotection: advancing the concept of reverse cholesterol transport. *Circulation.* **125:** 1905–1919.

8. Heinecke, J. W. 2012. The not-so-simple HDL story: a new era for quantifying HDL and cardiovascular risk? *Nat. Med.* **18:** 1346–1347.

9. Fang, L., S. H. Choi, J. S. Baek, C. Liu, F. Almazan, F. Ulrich, P. Wiesner, A. Taleb, E. Deer, J. Pattison, et al. 2013. Control of angiogenesis by AIBP-mediated cholesterol efflux. *Nature.* **498:** 118–122.

10. Mao, R., S. Meng, Q. Gu, R. Araujo-Gutierrez, S. Kumar, Q. Yan, F. Almazan, K. A. Youker, Y. Fu, H. J. Pownall, et al. 2017. AIBP limits angiogenesis through gamma-secretase-mediated upregulation of Notch signaling. *Circ. Res.* **120:** 1727–1739.

11. Zhang, M., L. Li, W. Xie, J. F. Wu, F. Yao, Y. L. Tan, X. D. Xia, X. Y. Liu, D. Liu, G. Lan, et al. 2016. Apolipoprotein A-1 binding protein promotes macrophage cholesterol efflux by facilitating apolipoprotein A-1 binding to ABCA1 and preventing ABCA1 degradation. *Atherosclerosis.* **248:** 149–159.

12. Ritter, M., C. Buechler, A. Boettcher, S. Barlage, A. Schmitz-Madry, E. Orso, S. M. Bared, G. Schmiedeknecht, C. H. Baehr, G. Fricker, et al. 2002. Cloning and characterization of a novel apolipoprotein A-I binding protein, AI-BP, secreted by cells of the kidney proximal tubules in response to HDL or ApoA-I. *Genomics.* **79:** 693–702.

13. Bodnar, J. S., A. Chatterjee, L. W. Castellani, D. A. Ross, J. Ohmen, J. Cavalcoli, C. Wu, K. M. Dains, J. Catanese, M. Chu, et al. 2002. Positional cloning of the combined hyperlipidemia gene Hyplip1. *Nat. Genet.* **30:** 110–116.

14. Westerfield, M. 2007. The Zebrafish Book. A Guide for the Laboratory Use of Zebrafish (*Danio rerio*). 5th edition. University of Oregon Press, Eugene, OR.

15. Fang, L., S. R. Green, J. S. Baek, S. H. Lee, F. Ellett, E. Deer, G. J. Lieschke, J. L. Witztum, S. Tsimikas, and Y. I. Miller. 2011. In vivo visualization and attenuation of oxidized lipid accumulation in hypercholesterolemic zebrafish. *J. Clin. Invest.* **121:** 4861–4869.

16. Kim, J. H., S. R. Lee, L. H. Li, H. J. Park, J. H. Park, K. Y. Lee, M. K. Kim, B. A. Shin, and S. Y. Choi. 2011. High cleavage efficiency of a 2A peptide derived from porcine teschovirus-1 in human cell lines, zebrafish and mice. *PLoS One.* **6:** e18556.

17. Tsimikas, S., A. Miyanohara, K. Hartvigsen, E. Merki, P. X. Shaw, M. Y. Chou, J. Pattison, M. Torzewski, J. Sollors, T. Friedmann, et al. 2011. Human oxidation-specific antibodies reduce foam cell formation and atherosclerosis progression. *J. Am. Coll. Cardiol.* **58:** 1715–1727.

18. Choi, S. H., P. Wiesner, F. Almazan, J. Kim, and Y. I. Miller. 2012. Spleen tyrosine kinase regulates AP-1 dependent transcriptional response to minimally oxidized LDL. *PLoS One.* **7:** e32378.

19. Raetz, C. R., T. A. Garrett, C. M. Reynolds, W. A. Shaw, J. D. Moore, D. C. Smith, Jr., A. A. Ribeiro, R. C. Murphy, R. J. Ulevitch, C. Fearns, et al. 2006. Kdo2-Lipid A of *Escherichia coli*, a defined endotoxin that activates macrophages via TLR-4. *J. Lipid Res.* **47:** 1097–1111.

20. Huang, X., A-V. Hartley, Y. Yin, J. H. Herskowitz, J. J. Lah, and K. J. Ressler. 2013. AAV2 production with optimized N/P ratio and PEI-mediated transfection results in low toxicity and high titer for in vitro and in vivo applications. *J. Virol. Methods.* **193:** 270–277.

21. Sears, D. D., P. D. Miles, J. Chapman, J. M. Ofrecio, F. Almazan, D. Thapar, and Y. I. Miller. 2009. 12/15-Lipoxygenase is required for the early onset of high fat diet-induced adipose tissue inflammation and insulin resistance in mice. *PLoS One.* **4:** e7250.

22. Whetzel, A. M., J. M. Sturek, M. H. Nagelin, D. T. Bolick, A. K. Gebre, J. S. Parks, A. C. Bruce, M. D. Skaflen, and C. C. Hedrick. 2010. ABCG1 deficiency in mice promotes endothelial activation and monocyte-endothelial interactions. *Arterioscler. Thromb. Vasc. Biol.* **30:** 809–817.

23. O'Connell, B. J., M. Denis, and J. Genest. 2004. Cellular physiology of cholesterol efflux in vascular endothelial cells. *Circulation.* **110:** 2881–2888.

24. Stoletov, K., L. Fang, S. H. Choi, K. Hartvigsen, L. F. Hansen, C. Hall, J. Pattison, J. Juliano, E. R. Miller, F. Almazan, et al. 2009. Vascular lipid accumulation, lipoprotein oxidation, and macrophage lipid uptake in hypercholesterolemic zebrafish. *Circ. Res.* **104:** 952–960.

25. Kim, F., M. Pham, E. Maloney, N. O. Rizzo, G. J. Morton, B. E. Wisse, E. A. Kirk, A. Chait, and M. W. Schwartz. 2008. Vascular inflammation, insulin resistance, and reduced nitric oxide production precede the onset of peripheral insulin resistance. *Arterioscler. Thromb. Vasc. Biol.* **28:** 1982–1988.

26. Hartvigsen, K., C. J. Binder, L. F. Hansen, A. Rafia, J. Juliano, S. Horkko, D. Steinberg, W. Palinski, J. L. Witztum, and A. C. Li. 2007. A diet-induced hypercholesterolemic murine model to study atherogenesis without obesity and metabolic syndrome. *Arterioscler. Thromb. Vasc. Biol.* **27:** 878–885.

27. Chung, S., J. K. Sawyer, A. K. Gebre, N. Maeda, and J. S. Parks. 2011. Adipose tissue ATP binding cassette transporter A1 contributes to high-density lipoprotein biogenesis in vivo. *Circulation.* **124:** 1663–1672.

28. de Haan, W., A. Bhattacharjee, P. Ruddle, M. H. Kang, and M. R. Hayden. 2014. ABCA1 in adipocytes regulates adipose tissue lipid content, glucose tolerance, and insulin sensitivity. *J. Lipid Res.* **55:** 516–523.

29. Choi, S. H., and H. N. Ginsberg. 2011. Increased very low density lipoprotein (VLDL) secretion, hepatic steatosis, and insulin resistance. *Trends Endocrinol. Metab.* **22:** 353–363.

30. Laatsch, A., M. Merkel, P. J. Talmud, T. Grewal, U. Beisiegel, and J. Heeren. 2009. Insulin stimulates hepatic low density lipoprotein receptor-related protein 1 (LRP1) to increase postprandial lipoprotein clearance. *Atherosclerosis.* **204:** 105–111.

31. Wada, J., and H. Makino. 2016. Innate immunity in diabetes and diabetic nephropathy. *Nat. Rev. Nephrol.* **12:** 13–26.

32. Lawrence, T., and G. Natoli. 2011. Transcriptional regulation of macrophage polarization: enabling diversity with identity. *Nat. Rev. Immunol.* **11:** 750–761.

33. Płóciennikowska, A., A. Hromada-Judycka, K. Borzecka, and K. Kwiatkowska. 2015. Co-operation of TLR4 and raft proteins in LPS-induced pro-inflammatory signaling. *Cell. Mol. Life Sci.* **72:** 557–581.

34. Jha, K. N., I. A. Shumilin, L. C. Digilio, O. Chertihin, H. Zheng, G. Schmitz, P. E. Visconti, C. J. Flickinger, W. Minor, and J. C. Herr. 2008. Biochemical and structural characterization of apolipoprotein A-I binding protein, a novel phosphoprotein with a potential role in sperm capacitation. *Endocrinology.* **149:** 2108–2120.

35. Shumilin, I. A., M. Cymborowski, O. Chertihin, K. N. Jha, J. C. Herr, S. A. Lesley, A. Joachimiak, and W. Minor. 2012. Identification of unknown protein function using metabolite cocktail screening. *Structure.* **20:** 1715–1725.

36. Marbaix, A. Y., G. Noël, A. M. Detroux, D. Vertommen, E. Van Schaftingen, and C. L. Linster. 2011. Extremely conserved ATP- or ADP-dependent enzymatic system for nicotinamide nucleotide repair. *J. Biol. Chem.* **286:** 41246–41252.